The source of the 30 October 1930, M_w 5.8, *Senigallia* (central Italy) earthquake: a convergent solution from instrumental, macroseismic and geological data

Paola Vannoli[1*], Gianfranco Vannucci[2], Fabrizio Bernardi[1], Barbara Palombo[1], Graziano Ferrari[2]

(1) Istituto Nazionale di Geofisica e Vulcanologia, sezione Roma 1, Via di Vigna Murata, 605, I-00143, Rome, Italy

(2) Istituto Nazionale di Geofisica e Vulcanologia, sezione di Bologna, Via Donato Creti, 12, I-40127, Bologna, Italy

[*] Corresponding author

Electronic Supplement collects methods, data and elaborations to make transparent the seismotectonic characterization. In particular it provides a short description of the method used for moment tensor computation, all the available focal mechanisms, the list of the available stations, with specification of those used or not used for hypocenter and moment tensor computation, maps of seismic flux showing areas of larger energy release, and detailed maps of the uncertainties for each realization of the macroseismic epicenter.

Abstract

On 30 October 30 1930 a M_w 5.8 earthquake hit the northern Marche coastal area (central Italy), causing significant damage (I_o VIII-IX degree MCS) along a 40 km stretch of the Adriatic coast between Pesaro and Ancona centered on the town of Senigallia. This area is characterized by relatively infrequent and moderate-size earthquakes and by elusive active faults. In spite of the presence of well-known NW-SE trending, NE verging fault-propagation folds forming the outer thrusts of the Apennines, the current state of activity and the kinematics of these coastal structures is still controversial.

We present a multidisciplinary analysis of the source of the 30 October 1930 *Senigallia* earthquake, combining instrumental and macroseismic data and elaborations with available evidence from geological and tectonic investigations. We determine the main seismic parameters of the source, including the earthquake location, its magnitude, and for the first time, its focal mechanism, providing the first instrumental evidence for thrust faulting along the northern Marche coastal belt.

Our findings have significant implications for the seismic hazard of the northern Marche coastal area, a densely populated region that hosts historical and monumental heritage, tourism facilities, industrial districts and key transportation infrastructures.

INTRODUCTION

Damaging earthquakes are often the only means of understanding the tectonics and assessing the seismogenic potential of areas of great geodynamic complexity. Due to its elusive active faults and relatively infrequent earthquakes, Italy is indeed one of such areas. Reliable source information is generally available for earthquakes of M≥5.5 that occurred after the inception of the WWSSN (World-Wide Standardized Seismic Network) in the early 1960s, i.e. over 60 years following the establishment of the first modern observatories at the end of the 19th century; yet many key earthquakes occurred in the early instrumental era, i.e. during those 60 years, and were hence recorded by the sparse and heterogeneous seismometers of the time.

Earthquakes of the first half of the 20th century era have been traditionally and rather successfully investigated through their macroseismic signature, i.e. based on the distribution of their effects quantified by macroseismic intensity (e.g. Postpischl, 1985; Levret *et al*., 1994; Bakun and Wentworth, 1997; Gasperini *et al*., 1999, 2010). More recently several investigators attempted to derive their essential source parameters, including the earthquake location, magnitude and focal mechanism, by carefully retrieving, processing and analyzing all available seismograms (e.g. Baroux *et al.*, 2003 for the 1909, *Lambesc* earthquake, southern France; Stich *et al.*, 2005, for the 1909 *Benavente* earthquake, central Portugal; Pino *et al*., 2008, for the 1930 *Irpinia* earthquake, southern Italy; Pino *et al*., 2009, for the 1908 *Messina Straits* earthquake, southern Italy; Bernardi *et al*., submitted, for the 1917 *Monterchi* earthquake, central Italy). In all cases the intensity-and instrumentally-derived parameters were compared with available tectonic, stress field and GPS evidence. All in all, the joint analysis of macroseismic, instrumental and tectonic evidence has turned out to be a promising tool for unveiling the characteristics of these rather elusive earthquakes, providing robust information to be used for

67 building improved seismogenic models, and ultimately for obtaining more reliable seismic
68 hazard analyses.
69 In this paper we combined instrumental and macroseismic evidence for the 30 October 1930,
70 *Senigallia*, central Italy earthquake (estimated M_w prior to this work: 5.81, I_o=VIII-IX MCS; see
71 CPTI11, Data and Resources Section), with available evidence from geological and tectonic
72 investigations. Positively identifying large active faults and assigning historical earthquakes to
73 each of them is a difficult and often challenging task over much of Italy, and the 1930
74 earthquake is well representative of this condition. Difficulties arise from the predominance of
75 blind faulting combined with the presence of inherited tectonic landscape and with the relatively
76 low rates of present tectonic deformation (see Valensise and Pantosti, 2001a, and Vannoli *et al*.,
77 2012, 2014, among several others).
78 The 1930 earthquake hit at 7:13:06 UTC, bringing destruction to a large stretch of the
79 northern Marche coastal area between Pesaro and Ancona (Oddone, 1930; Favali *et al*., 1995;
80 CFTI4Med, see Data and Resources Section; Fig. 1). It killed 18 people, injured many more and
81 caused widespread property damage, leaving hundreds of people homeless (Fig. 2). It was felt
82 over a rather large area (inset in Fig. 2), perhaps due to the low attenuation properties at crustal
83 scale of the Adriatic region (Carletti and Gasperini, 2003). The earthquake was followed by a
84 sizeable tsunami (I=4; *strong*, according to the Sieberg-Ambraseys scale; Pasarić *et al*., 2012)
85 that flooded the Ancona coastline and was detected by all crews in the city harbor (CFTI4Med,
86 see Data and Resources Section). Only two direct witnesses are available from Ancona and from
87 Bakar (see A and B, respectively, in inset of Fig. 2; Pasarić *et al*., 2012). Therefore, the
88 information on the tsunami is surprisingly limited considering a) the extent of the Adriatic Sea
89 coasts potentially exposed to it, b) the distance between the two cities (about 200 km), and c)
90 that Bakar is located in a embayment protected by the presence of islands parallel to the coast
91 (inset in Fig. 2).

The 30 October 1930 *Senigallia* earthquake is crucial for a better understanding of the seismic hazard of the northern Adriatic coastal belt. We aimed at improving the knowledge on its source based on the comparison of three end members, namely macroseismic, instrumental and geological data and elaborations (Table 1).

SEISMOTECTONIC FRAMEWORK

The northern Marche coastal area lies on the eastern side of the Apennines range. The Apennines comprise a typical fold-and-thrust belt that developed in Neogene and Quaternary times at the hangingwall of a west-directed subduction zone. Over time the Apennines compressional domain migrated towards the northeast as a response to the progressive roll-back of the Adriatic lithosphere (e.g. Malinverno and Ryan, 1986). The outer thrusts of the Apennines propagated towards the Adriatic offshore, resulting in a complex pattern of NW-SE trending anticlines and NE-verging thrust faults and backthrusts running parallel to the coastline (Fig. 3). Due to its significant hydrocarbon potential the region has been thoroughly investigated using commercial seismic reflection profiles, but the literature offers substantially different interpretations for the architecture of its thrust system. The main differences concern the position of the basal *decollement* of the thrusts and the presence of secondary shallower *decollement* levels (thin-skinned vs thick-skinned structural style; e.g. Bally *et al*., 1986; Barchi *et al*., 1998). According to the recent work by Maesano *et al*. (2013), the deeper detachment (having a depth of 6-10 km) controls the development of anticlines bounded by major thrust ramps. Overall the tectonic activity of the area is characterized by the interplay of the described thrust-faults and a number of ENE-WSW-trending, sub-vertical faults known as "transverse structures" (Fig. 3). These exhibit relatively unclear kinematics but are likely to represent regional-scale tear faults that accommodate strain between different portion of the thrust system (Kastelic *et al*., 2013).

In spite of this relatively clear tectonic framework, the current state of activity and the kinematics of the coastal tectonic structures that may be responsible for the 1930 earthquake and for other events that occurred between Rimini and Ancona is still controversial. Based on the presumed lack of evidence for compressional deformation in post-Early Pleistocene offshore deposits, different investigators suggested that thrusting and folding ended in the Early Pleistocene (Coward *et al*., 1999; Di Bucci and Mazzoli, 2002), and that current activity is dominated by extensional or strike-slip faulting (Macchiavelli *et al*., 2012; Mazzoli *et al*., 2014). Based on geological and geomorphological evidence and on the ongoing seismicity, other investigators maintained that the coastal folds are growing, and therefore that the underlying thrust fronts are still active (Vannoli *et al*., 2004; Scrocca, 2006; Basili and Barba, 2007). As a result of this interpretation, the blind thrust-faults located at the leading-edge of the Apennines accretionary prism are considered the main seismogenic sources in the area (seismogenic sources were obtained from the Database of Individual Seismogenic Sources (DISS), Version 3.1.1, see Data and Resources Section; Basili *et al*., 2008; Fig. 3). A recent re-analysis of seismic lines by Maesano *et al*. (2013) led to the identification of growth strata within youthful units, supporting the activity of the most external thrust fronts and allowing their strain rates to be assessed with great accuracy. Finally, Mazzoli *et al.* (2014) used evidence from an earthquake sequence that occurred off the coast of Numana in June 2013 (max M_w 4.9) to suggest that the area is characterized by the occurrence of active strike-slip faults dissecting the thrust belt.

Figure 4 shows the seismicity of the study area for the period 1981 to present, taken from a recent instrumental catalogue (Gasperini *et al*., 2012; Gasperini *et al*., 2013a, 2013b; Lolli *et al*, 2014). The earthquake record is extended back in time up to 1005 A.D. by the CFTI catalogue (Guidoboni *et al.*, 2007), the CPTI11 catalogue (see Data and Resources Section) and the ISC Bulletin (see Data and Resources Section). Seismicity occurs dominantly along two subparallel belts striking NW-SE, one elongated following the Apennines axis, the other one straddling the Adriatic coast up to 10-15 km offshore (Fig. 4a). Most large historical earthquakes such as 1930

occurred along this belt, whereas the area between the Apennines and the coastline appears almost completely silent.

Focal mechanisms are a robust indicator of coseismic strain and provide information on the local tectonic style. The few solutions available for the Marche coastal area (Pondrelli *et al.*, 2002, 2011; Vannucci and Gasperini, 2003, 2004; Vannucci *et al*., 2010; Scognamiglio *et al.*, 2009; for a complete list and representation of focal mechanisms, see Table S1 in the *Electronic supplement*) delineate an area of dominantly strike-slip faulting about 5 km off the coast between Senigallia and Ancona and a belt undergoing compression running inland, 10-20 km from the coastline. Compressional and strike-slip faulting hence coexist in the study area as both are coherent with the mean direction of the P and T axes (Fig. 3). The P axis direction is in agreement with the SHmax direction retrieved from stress data (Fig. 4a; Heidbach *et al*., 2008) and is perpendicular to the orientation of the main structural elements (anticlines and thrust fronts). GPS data available for the northern Marche area display a general reduction of horizontal velocities with respect to fixed Eurasia along a NE-SW trend, suggesting active compression and shortening perpendicular to the coastline (e.g. Devoti *et al*., 2011).

In summary, the active tectonics record of the northern Marche coastal region is still rather controversial, and the limited evidence from focal mechanisms, *stress-in-situ* and GPS data does not allow to put firm constraints on one tectonic scenario or the other. All of these reasons make investigating the source of the 1930 earthquake a crucial step towards a full understanding of the local tectonic framework and of a careful assessment of the associated earthquake potential.

DEFINITION OF THE SEISMOGENIC SOURCE

From geological and tectonic data

169 The source of the 1930 earthquake has been investigated since the early stages of the
170 compilation of the DISS database (see Data and Resources Section; Valensise and Pantosti;
171 2001b), also in the framework of a specific multidisciplinary investigation of the seismic hazard
172 and seismic response of the town of Senigallia and its surroundings (Mucciarelli and Tiberi,
173 2007). The hypotheses put forward in the DISS database are based on the observation of active
174 growth of the coastal anticlines of the northern Marche coast. The proposed source, referred to
175 here as Geological Source (GS), corresponds with a blind thrust-fault (Fig. 3) detected by
176 geophysical prospecting (e.g. Bally *et al*., 1986; Fantoni and Franciosi, 2010) and causing a
177 distinct signature in the evolution of the coastal landscape. Vannoli *et al*. (2004) investigated the
178 drainage and coastal system and their associated features (channel migrations/avulsions,
179 raised/warped terraces, bedding attitude) along the entire northern Marche coastal belt. They
180 analyzed anomalous drainage patterns and deformed Middle-Late Pleistocene alluvial and
181 coastal terraces, identifying, mapping and correlating with past sea-levels a continuous sequence
182 of alluvial and coastal terraces. They found out that terrace treads are consistently warped,
183 suggesting that in order to produce a significant vertical displacement of the seafloor and
184 generate the observed tsunami, the fault responsible for the *Senigallia* earthquake must be very
185 close to the coast or offshore. In fact, the DISS database assumes the entire blind thrust front
186 from Pesaro to Ancona to be an active and potentially seismogenic system (Fig. 3).
187 In detail, the width (7 km) of the GS is based on evidence from seismic reflection profiles,
188 while its length (12 km) is constrained on the basis of major fluctuations of the fold axial-plane
189 (Vannoli *et al*., 2004). Based on empirical relationships (Wells and Coppersmith, 1994) this fault
190 size yields a "geological magnitude" M_w 5.9. The fault strike and dip are based on the general
191 trend of mapped surface structures and on subsurface data, respectively. The assigned rake
192 corresponds to pure thrusting, in agreement with the geodynamic considerations described in the
193 previous section. The minimum and maximum depth (4.0-7.5 km, respectively) are based on
194 subsurface data. Geomorphic markers and growth strata yield slip rate values of 0.24-0.36 mm/y

(Vannoli *et al*., 2004) and 0.37-0.52 mm/y (Maesano *et al*., 2013), respectively for the Upper Pleistocene and for the Plio-Pleistocene. We qualitatively investigated the surface effects of the GS through standard dislocation modeling of a blind fault embedded in an elastic half-space (Okada, 1985), and found that the expected vertical displacement of the hangingwall (Fig. 3) is consistent with geomorphological evidence and with the generation of a ~~small~~ tsunami.

From the analysis of macroseismic data

Italy is blessed with the existence of mature and especially rich macroseismic databases resulting from the pioneering work of local historical seismologists (CFTI4Med; CPTI11, see Data and Resources Section). These data have been routinely used to derive reliable source parameters for hundreds of pre-instrumental or early-instrumental earthquakes although open issues still survive, for instance on the determination of focal depth and on the correct location of offshore events.

We used the BOXER code (Gasperini *et al*., 1999, 2010) to derive the essential parameters of the 1930 earthquake source (location, magnitude, source orientation and source size) from its macroseismic signature, that is to say, a true Macroseismic Source (MS). Boxer supplies also estimates of the reliability of such parameters, expressed by formal and empirical uncertainties. The latest release of the code provides seven different methods for calculating the macroseismic epicenter (numbered from 0 to 6 in Table 2, Fig. 5, and Fig. S2 of *Electronic supplement*). Method #0 ("barycenter") is based on the area of the largest intensities, whereas methods #1-6 ("radiation center"), are based on the maximization of the likelihood function of a log-linear "extended" attenuation equation (Pasolini *et al*., 2008), with 6 unknown parameters (epicentral latitude and longitude, hypocentral depth, epicentral intensity, linear and logarithm part of the attenuation equation), using the observed intensity data. Methods #1-6 always estimate the epicenter location (latitude and longitude) and some, by different combinations, or all the other parameters (see Gasperini *et al*., 2010 for further details). Formal uncertainties are the standard

deviation of the parameter averages for method #0, and the variance/covariance matrix for methods #1-6, obtained by inverting the finite-difference Hessian of the likelihood function at its maximum (Guo and Ogata, 1997). Bootstrap simulations (Efron and Tbishirani, 1986; Hall, 1992) allow the empirical uncertainties to be quantified using a variance/covariance matrix and 240 Bootstrap Para-Data (BPDs) sets of the intensity dataset. Very small formal and bootstrap uncertainties reduce the dispersion from the measures and are a robust estimator of the reliability and stability of the parameters obtained.

Figure 5 shows a summary of the macroseismic locations obtained. They are rather distant from each other: locations of for methods #0-4 fall onshore within a ~3 km long area and the associated uncertainties are small, whereas those obtained with methods #5 and #6 fall offshore with relatively large uncertainties (Table 2 and Fig. 5). The availability of 7 macroseismic epicenters, two of which located offshore, requires an *a priori* decision on whether the epicenter of the 1930 earthquake has a higher probability of being located inland or offshore. For previous events analyzed by Gasperini *et al*. (2010) and known to have occurred offshore, methods #1-6 have all shown a tendency to shift the epicenter offshore and all exhibit similar uncertainties. We therefore suggest that most likely the *Senigallia* earthquake occurred inland. Methods #5 and #6 are the most sensitive to the shifts of the epicenter since the specific calibration of the parameters of the logarithmic and/or linear parts of the attenuation law improves the fit with the entire distribution of the macroseismic data. Hence to fit the distribution of all observed intensities, which is strongly asymmetric due to the presence of the Adriatic Sea and to the lack of data from its opposite (Croatian) shores (Fig. 2), the epicenters tend to shift offshore perpendicular to the coast.

We then used BOXER to compute the macroseismic magnitude, again based on the attenuation equation of Pasolini *et al*. (2008; Table 2 and Fig. 5). All methods (#0-6) provide similar magnitudes (M_w 5.8$\pm$0.1) that are only slightly lower than the M_w obtained by other investigators (e.g. CPTI11, see Data and Resources Section).

To compute the source ("box") azimuth BOXER uses a “weighted axial mean” of the distribution of the axial orientations with respect to the earthquake location, using only the datapoints where the highest intensities were reported, i.e. the “near field” of the macroseismic distribution, which includes the localities closest to the seismogenic fault where the ground shaking is greatest due to the physical extent of the rupture. The resulting azimuth (121.4°; Fig. 5) was obtained with method #0; this is the only method that could be used, considering that the alternative epicenters (methods #1-6) are anyway shifted with respect to the highest observed intensities. Although the distribution of intensities is asymmetric due to lack of intensities toward the northeast (i.e. beyond the coastline), BOXER allows a reliable computation of the fault orientation because the epicenter is inland or very close to the coastline. Conversely, when the epicenter is offshore the source radiation pattern is poorly defined and the source azimuth is indefinite because BOXER expects the intensity data to be more or less evenly distributed. As stated earlier on, we believe the inland locations supplied by methods #0-4 are reliable. For computing azimuth (method #0) BOXER uses 13 highest intensities (12 sites with intensity VIII MCS and one with VIII-IX) spread over a relatively large search area.

The stability and reliability of the macroseismic solution for the orientation of the prospective causative fault of the 1930 earthquake is statistically significant because: 1) the Rayleigh and Kuiper (Rock, 1988; Fisher, 1993) tests yield < 0.1, which implies rejecting the assumption of uniform distribution; 2) the distribution of the frequency of occurrence for all BPDs is very narrow and there are almost no outliers; 3) formal (±1.4°) and bootstrap (±4.3°) uncertainties are small. The computed orientation is also roughly similar to the principal axis of the epicentral ellipse uncertainties for methods #0-4 (Fig. 5). Gasperini *et al*. (2010) demonstrated a good correlation between the macroseismic-derived source orientations and the focal mechanisms available for Italian earthquakes, in particular those having M≥5.7. By assuming the reliability of their associated statistics, the computed macroseismic orientation has an 80% probability of representing the true strike of the earthquake causative fault, within a confidence range of 10°.

Finally, we combine the macroseismic-derived magnitude and source orientation with the empirical relations of Wells and Coppersmith (1994) to derive for the *Senigallia* macroseismic source (MS; Fig. 5) a length and a width of 10.2 and 6.4 km, respectively.

Earthquake parameters from the analysis of historical seismograms

Early instrumental estimates of the hypocenter of the 1930 earthquake were supplied by the International Seismological Summary (ISS, see Data and Resources Section) and by Gutenberg and Richter (GUTE; 1954). The ISS hypocenter falls near Ancona while the GUTE hypocenter is located 10 km offshore, between Senigallia and Ancona, at 35 km depth (Fig. 5). The GUTE location, however, is admittedly approximated to the nearest 1/4 of degree, both in latitude and longitude. The ISS bulletin reports 91 stations for which arrival times are available (64 P and 49 S phases: Table 3 and Table S2 in the *Electronic supplement*). Both ISS and GUTE do not provide location uncertainties.

The SISMOS project (http://sismos.ingv.it/en/) was initiated in 2001 by INGV scientists. It involves scanning, archiving and distributing historical seismograms, station bulletins, log books and related information retrieved from Italian observatories and dating as far back as 1895 (Michelini *et al.*, 2005). SISMOS has already retrieved and processed seismograms written by about a thousand strong earthquakes that occurred in the Euro-Mediterranean area from the early 20^{th} century.

For the 30 October 1930 earthquake the SISMOS database supplies 113 high resolution scans of the seismograms recorded at 34 different stations (Table 4 and Table S2 in the *Electronic supplement*); time corrections for most of these seismograms are not available. The ISS bulletin collects 132 P and S phases of 90 stations. Therefore we used the data from the ISS Bulletin to locate the earthquake epicenter and a set of historical seismograms to assess its focal mechanism and magnitude.

298 To relocate the 1930 earthquake and estimate the associated location uncertainty ellipse at
299 90% confidence (Fig. 5) we used the fully non-linear earthquake location package NonLinLoc
300 (NLL; Lomax, 2005) with an Equal-Differential-Time (EDT) misfit function. The code performs
301 a probabilistic location of the hypocenter (Fig. 5), quantified by a Probability Density Function
302 (PDF) in a 3D space. The PDF is obtained by means of an equal differential-time formulation of
303 the likelihood function, containing the calculated and observed differences between two stations,
304 summed over all observations pairs. We adopted the model AK135 (Kennet, 2005) for
305 teleseismic phases and a standard Italian crustal model (Basili *et al*., 1984) for local phases.
306 The NLL procedure converges to the final solution (Lon: 13.45°, Lat: 43.87°) after 5
307 iterations, using 35 phases (21 P and 14 S) and 29 stations (of the 91 available), with a maximum
308 azimuthal gap of 48 degrees (Table 3, Figs. 5 and 6). This gap increases to about 100 degrees if
309 we take into account only stations located in an area centered on the epicenter and having a
310 radius of 700 km (not considering three stations located about 1,600 km away, in Crimea: SEV,
311 SIM, and YAL, see Fig. 6). Arrival phases were automatically and manually re-associated, and
312 the outliers were eliminated at each iteration. Thanks to the definition of the EDT function
313 (Lomax, 2005), however, the method is not much sensitive to the presence of outliers.
314 We then computed the focal mechanism and earthquake magnitude by a formal Moment
315 Tensor (MT) inversion. Due to the instrument response and to the quality of data recording, the
316 procedure used for earthquakes recorded by historical seismographs is significantly different
317 from the procedure used for modern events. More specifically, the MT inversion of old
318 seismograms must face difficulties arising from: i) the static magnification, which in general is
319 significantly smaller than for modern digital broadband seismometers, causing smaller
320 amplitudes and less waveform details; ii) the irregular speed of the seismograph's drum, which
321 introduces velocity phase distortions in the seismograms; iii) fast motion of the seismograph's
322 nib that causes weak or absent traces on the recordings of stations close to the epicenter iv) the
323 inaccurate synchronization of the station clock used for reading arrival times; and v) the limited

frequency range response and short periods of seismographs: 1-20 and 10-30 seconds for mechanical and electromagnetic instruments, respectively (Bernardi *et al*., 2005).

Fifteen stations (Table 4) provided seismograph traces potentially useful for the MT computation of the 1930 event. We used 12 power spectra amplitudes (from 11 stations) and 19 first P-phase arrival polarities (from 13 stations) to constrain the P- and T-axes. The calculation is based on the method proposed by Bernardi *et al*. (submitted; see the *Electronic supplement*) and on 5,000 synthetic MTs from a Montecarlo simulation. The method is independent from the location of the epicenter in a range of ~20 km and allows the MT to be computed also for historical earthquakes, including poorly constrained and highly uncertain ones.

The best-fitting MT solution among all generated synthetic MTs, i.e. the solution corresponding to the minimum value of variance, is dominantly compressional but exhibits a minor strike-slip component (strike, dip and rake are 148°-36°-139° and 273°-68°-61°, respectively for plane 1 and plane 2; Fig. 7). The inferred magnitude is M_w 5.6, to be compared with the M_s 6.0 estimate of the International Seismological Summary (Villaseñor and Engdahl, 2005, from the Pasadena station) and with the M_s 5.97 (±0.39) estimate supplied by Margottini *et al*. (1993).

DISCUSSION AND CONCLUSIONS

We characterized the source of the 1930 earthquake by obtaining and comparing a Geological Source (GS), a Macroseismic Source (MS), a standard instrumental relocation and a MT solution for its magnitude and focal mechanism. The MT solution in particular is a key and original result of this study, based on the processing of pre-WWSSN seismograms with the amplitude spectra method (Bernardi *et al*., submitted; see the *Electronic supplement*), and shows a reverse fault with a minor strike-slip component.

First and foremost, the focal mechanism provides new additional constraints on the controversial current state of activity of the northern Marche coastal area. According to this mechanism, a thrust fault is responsible for the occurrence of the most significant earthquake that has struck the coastal region between Pesaro and Ancona historically. The new solution is coherent with the observed active compression and thrust kinematics seen along coastal tectonic structures (Vannoli *et al*., 2004), with the direction of maximum compression axis on the horizontal plane (Heidbach *et al.*, 2008) and with GPS velocities (Devoti *et al*., 2011). No direct clue is available to choose one of the two nodal planes of the focal mechanism, but most likely the fault responsible for the *Senigallia* earthquake is one of the relatively large, main NE-verging thrusts and not a secondary structure related to a SW-verging backthrust.

The MT method, the geological analysis, and the Boxer code (Gasperini *et al*., 2010) provided a range of magnitudes (5.6-5.9; Fig. 8) that are in good agreement with previous estimates (CPTI11, see Data and Resources Section: M_w 5.81; CFTI4Med, see Data and Resources Section: M_e 5.8±0.1, Margottini *et al*., 1993: M_s 5.97±0.39). Such fluctuations are well explained by the different data and methods used and also by the different types of magnitude available:

- the solution proposed by Margottini *et al*. (1993) is an M_s obtained from a reappraisal of magnitudes from bulletins;
- the "geological magnitude" was calculated using an empirical relationship (Kanamori and Anderson, 1975; Wells and Coppersmith, 1994) based on geological evidence. According to Vannoli *et al*., (2004), the observed deformation of the fluvial and coastal terraces is compatible with a ~12 km-long fault, yielding M_w 5.9. Being based on long-term geological observations, however, this estimate should be regarded as a maximum.
- the solution obtained from macroseismic observations using the BOXER code is M_w 5.8+0.1. This estimate should be considered equivalent to M_w since the earthquakes used for calibration are events for which an instrumental M_w is available;

- the M_w from MT is directly computed from seismograms after correction for the poles and zeros of the instruments. However, the M_w 5.6 computed from MT is lower than the magnitudes derived from both geological and macroseismic observations. This may be due to the behavior of the mechanical seismometers, which act like a high-pass filter and exhibit very low sensitivity to phases with periods of 20 seconds or longer. For this reason and since the macroseismic (M_w 5.8±0.1) and the geological (M_w 5.9) magnitudes are consistent with each other, we set our preferred magnitude to M_w 5.8±0.1.

The MT inversion method (Bernardi *et al*., submitted) does not discriminate among all possible hypocentral locations within a radius of ~20 km, implying that the MT solution is compatible with both a blind thrust located close the coast and with a fault offshore (Fig. 3). Both these potential sources may generate enough vertical displacement of the sea floor to explain the tsunami observations in Ancona. As for Bakar, we maintain that the account by Pasarić *et al*. (2012) is unreliable and that propagation of the 1930 tsunami across the entire Adriatic Sea is rather unrealistic.

Gasperini *et al*. (2010) tested the correspondence between macroseismic and instrumental epicenters for post-WWSSN earthquakes, and found that ~60% agree within 10 km. This implies that the macroseismic location is reliable enough to be confidentially extended in time for older earthquakes. Methods #0-4 locate the epicenter in a narrow area along the coast, while only methods #5 and #6 place the epicenter offshore, near the NLL solution (Figs. 3 and 5). As discussed earlier, available oil industry profiles show a large and presumably active fault constrained in the 4.0-7.5 km depth interval below the area indicated by methods #0-4. The joint interpretation of the available evidence suggests that the 1930 was caused by a fault located inland but very close to the coast (in fact, the coast is believed to be controlled by fault activity), where the GS and MS sources are very close.

The instrumental location calculated with NLL falls ~20 km north of the macroseismic epicenter MS (Fig. 5). This is not surprising in view of the considerable uncertainties affecting

402 instrumental records from the first half of the 20th century, largely resulting from the sparseness
403 of the available stations and from their large epicentral distance. In addition to the intrinsic
404 limitations of old instrumental data (extensively discussed in Bernardi *et al*., submitted; *see the*
405 *Electronic Supplement*), the 1930 earthquake has the disadvantage of a poor azimuthal coverage
406 of the stations used by NLL, which exhibit a non-homogeneous distribution with a strong
407 concentration in the NW quadrant (see rose diagram in Fig. 5). Different location methods yield
408 different instrumental epicenters that are difficult to rank based on their reliability. The bottom
409 line is that, as noted by previous investigators (e.g. Pino *et al*., 2009), historical instrumental data
410 are crucial for assessing the magnitude and the focal mechanism of significant earthquakes of the
411 pre-WWSSN era, but macroseismic data are generally more robust for determining the
412 earthquake epicenter.

413 Figure 8 summarizes the geometrical and kinematic parameters of the MT, MS and GS
414 solutions, highlighting a good correspondence among the orientation of the MT preferred nodal
415 plane (148°), the strike of the GS (142°) and the strike of the MS (121°; Fig. 8). The dip of the
416 selected nodal plane of the MT (36°) is in good agreement with the dip of the thrust-fault
417 detected through geophysical prospecting (30°), subsequently adopted for the GS.

418 In summary, our results constrain the source of the 1930 earthquake as:

419 • being located close to the coast,
420 • at shallow crustal depth (between ~4.0 and ~7.5 km depth),
421 • striking parallel to the coast,
422 • dipping to the SW at ~30°,
423 • with dominantly thrust faulting kinematics.

424

425 The 1930 earthquake was hence caused by a shallow-dipping fault lying beneath one of the
426 NW-SE trending, NE verging fault-propagation folds of the Central Apennines thrust belt. This
427 implies that not only the northern Marche coastal thrust fronts are active, as suggested by

previous workers, but that they are also seismogenic and are likely to be responsible for all the largest historical earthquakes of the coastal belt. Not coincidentally, the source of the *Senigallia* earthquake is very similar to that of the 20 and 29 May 2012, Emilia earthquakes (M_w 6.1 and 6.0, respectively; see Anzidei *et al*., 2012, and papers therein), generated by faults lying beneath the westward prolongation of the same thrust fronts.

Our findings have strong implications for the seismic hazard of the densely populated northern Marche, a coastal region that hosts a number of monumental buildings, tourism facilities, industrial districts and key transportation infrastructures. The 1930 earthquake provides the first instrumental evidence for the activity of the frontal thrusts running beneath the present coastline. Similarly-sized thrusts have been identified as potential seismogenic sources by the DISS database v. 2.0 (Valensise and Pantosti, 2001b), both NW and SE of Senigallia (Fig. 3); two of them in particular, located near Fano and Pesaro, have been described as *potential seismic gaps* as they appear historically silent. Our findings show that a moderate-size earthquake (M_w<6.0) may represent a major threat for this region, suggesting that these quiescent seismogenic sources should be considered with special care.

Data and Resources

The Database of Individual Seismogenic Sources (DISS), Version 3.1.1 (doi: 10.6092/INGV.IT-DISS3.1.1.) was searched using http://diss.rm.ingv.it/diss/ (last accessed July 2014).

The Catalogue of Strong Earthquakes in Italy (461 B.C.-1997) and Mediterranean Area (760 B.C.-1500) (CFTI4Med) was searched using http://storing.ingv.it/cfti4med/ (last accessed July 2014).

The International Seismological Centre Bulletin (ISC) was searched using www.isc.ac.uk (last accessed December 2013).

The International Seismological Summary (ISS) was searched using http://storing.ingv.it/ISS/TIF/i30q4ind.html (last accessed March 2014).

The Parametric Catalogue of Italian Earthquakes (CPTI11; doi: 10.6092/INGV.IT-CPTI11) was searched using http://emidius.mi.ingv.it/CPTI (last accessed July 2014).

Acknowledgments

Comments of two anonymous reviewers helped improving the manuscript significantly. We wish to thank the *Aeronautica Militare Italiana* for the photographic material and two anonymous reviewers for their careful reviews. We are also especially grateful to Gianluca Valensise for constructive comments and suggestions.

References

Anzidei, M., A. Maramai, and P. Montone (Editors) (2012). The Emilia (northern Italy) seismic sequence of May-June, 2012: preliminary data and results, *Annals of Geophysics* **55**, no. 4.

Bakun, W. H., and C. M. Wentworth (1997). Estimating earthquake location and magnitude from seismic intensity data, *Bulletin of the Seismological Society of America* **87**, 1502-1521.

Bally, A. W., L. Burbi, C. Cooper, and R. Ghelardoni (1986). Balanced sections and seismic reflection profiles across the central Apennines, *Memorie della Società Geologica Italiana* **35**, 257-310.

Barchi, M., A. De Feyter, M. B. Magnani, G. Minelli, G. Pialli, and B. M. Sotera (1998). The structural style of the Umbria-Marche fold and thrust belt, *Memorie della Società Geologica Italiana* **52**, 557-578.

Baroux, E., N. A. Pino, G. Valensise, O. Scotti, and M. Cushing (2003). Source parameters of the 11 June 1909. Lambesc (Provence, southeastern France) earthquake: A reappraisal based

on macro- seismic, seismological, and geodetic observations, *J. Geophys. Res.* **108**, (B9), 2454, doi: 10.1029/2002JB002348.

Basili, A., G. Smriglio, and G. Valensise (1984). Procedure di determinazione ipocentrale in uso presso l'Istituto Nazionale di Geofisica, *Atti G.N.G.T.S.*, 875-884.

Basili, R., and S. Barba (2007). Migration and shortening rates in the northern Apennines, Italy: implications for seismic hazard, *Terra Nova* **19**, 462-468, doi: 10.1111/j.1365-3121.2007.00772.x.

Basili, R., G. Valensise, P. Vannoli, P. Burrato, U. Fracassi, S. Mariano, M. M. Tiberti, and E. Boschi (2008). The Database of Individual Seismogenic Sources (DISS), version 3: summarizing 20 years of research on Italy's earthquake geology, *Tectonophysics* **453**, 20-43, doi: 10.1016/j.tecto.2007.04.014.

Bernardi, F., J. Braunmiller, and D. Giardini (2005). Seismic Moment from Regional Surface-Wave Amplitudes: Applications to Digital and Analog Seismograms, *Bulletin of the Seismological Society of America* **95**, no. 2, 408-418, doi: 10.1785/0120040048.

Bernardi, F, M. G. Ciaccio, B. Palombo and G. Ferrari (*submitted*). Moment tensor inversion of early instrumental data: the application to the 1917 Monterchi earthquake, submitted to *Annals of Geophysics.*

Bigi, G., G. Bonardi, R. Catalano, D. Cosentino, F. Lentini, M. Parotto, R. Sartori, P. Scandone, and E. Turco (Editors) (1992). Structural Model of Italy 1:500,000, CNR Progetto Finalizzato Geodinamica.

Carletti, F., and P. Gasperini (2003). Lateral variations of seismic intensity attenuation in Italy, *Geophysical Journal International* **155**, 839-856.

Coltorti, M., and T. Nanni (1987). La bassa valle del Fiume Esino: geomorfologia, idrogeologia e neotettonica, *Bollettino della Società Geologica Italiana* **106**, 35-51.

Coward, M. P., M. De Donatis, S. Mazzoli, W. Paltrinieri, and F. C. Wezel (1999). Frontal part of the northern Apennines fold and thrust belt in the Romagna-Marche arc (Italy): Shallow and deep structural styles, *Tectonics* **18**, no. 3, 559-574.

Devoti, R., A. Esposito, G. Pietrantonio, A. R. Pisani, and F. Riguzzi (2011). Evidence of large scale deformation patterns from GPS data in the Italian subduction boundary, *Earth and Planetary Science Letters* **311**, 230-241, doi: 10.1016/j.epsl.2011.09.034.

Di Bucci, D., and S. Mazzoli (2002). Active tectonics of the northern Apennines and Adria geodynamics: new data and a discussion, *Journal of Geodynamics* **34**, 687-707.

Efron, B., and R. J. Tbishirani (1986). Bootstrap methods for standard errors, confidence intervals and other measures of statistical accuracy, *Statistical Science* **1**, 54-77.

Elmi, C., O. Nesci, D. Savelli, and G. Maltarello (1987). Depositi alluvionali terrazzati del margine adriatico appenninico centro-settentrionale: processi geomorfologici e neotettonica, *Bollettino della Società Geologica Italiana* **106**, 717-721.

Fantoni, R., and R. Franciosi (2010). Tectono-sedimentary setting of the Po Plain and Adriatic Foreland, *Rendiconti Fisica Accademia dei Lincei* **21**, no. 1, S197-S209, doi: 10.1007/s12210-010-0102-4.

Favali, P., F. Frugoni, D. Monna, M. L. Rainone, P. Signanini, and G. Smriglio (1995). The 1930 earthquake and the town of Senigallia (Central Italy): an approach to seismic risk evaluation, *Annali di Geofisica* **38**, no. 5-6, 679-689.

Fisher, N. I. (1993). *Statistical Analysis of Circular Data*, Cambridge University Press, Cambridge, United Kingdom, 277 pp.

Gasperini, P., F. Bernardini, G. Valensise, and E. Boschi (1999). Defining seismogenic sources from historical earthquake felt reports, *Bulletin of the Seismological Society of America* **89**, 94-110.

526 Gasperini, P., G. Vannucci, D. Tripone, and E. Boschi (2010). The location and sizing of
527 historical earthquakes using the attenuation of macroseismic intensity with distance, *Bulletin*
528 *of the Seismological Society of America* **100**, 5A, 2035-2066, doi: 10.1785/0120090330.
529 Gasperini, P., B. Lolli, G. Vannucci, and E. Boschi (2012). Calibration of moment magnitude
530 estimates for the European-Mediterranean and Italian regions, *Geophysical Journal*
531 *International* **190**, 1733-1745, doi: 10.1111/j.1365-246X.2012.05575.x.
532 Gasperini, P., B. Lolli, and G. Vannucci (2013a). Empirical Calibration of Local Magnitude Data
533 Sets Versus Moment Magnitude in Italy, *Bulletin of the Seismological Society of America*
534 **103**, no. 4, 2227-2246, doi: 10.1785/0120120356.
535 Gasperini, P., B. Lolli, and G. Vannucci (2013b). Body wave magnitude mb is a good proxy of
536 moment magnitude Mw for small earthquakes (mb<4.5-5.0), *Seismological Research Letters*
537 **84**, no. 6, 932-937, doi: 10.1785/0220130105.
538 Guidoboni, E., G. Ferrari, D. Mariotti, A. Comastri, G. Tarabusi, and G. Valensise (2007).
539 Catalogue of Strong Earthquakes in Italy from 461 BC. to 2000 and in the Mediterranean
540 area, from 760 BC. to 1500, An Advanced Laboratory of Historical Seismology,
541 http://storing.ingv.it/cfti4med/.
542 Guo, Z., and Y. Ogata (1997). Statistical relations between the parameters of aftershock in time,
543 space and magnitude, *Journal of Geophysical Research* **102**, 2857-2873.
544 Gutenberg, B., and C. F. Richter (1954). *Seismicity of the Earth and Associated Phenomena*,
545 Second Ed., Princeton University Press, NJ, 310 pp.
546 Hall, P. (1992). The *Bootstrap and Edgeworth Expansion*, Springer, New York, 372 pp.
547 Heidbach, O., M. Tingay, A. Barth, J. Reinecker, D. Kurfeß, and B. Müller (2008). The World
548 Stress Map database release, doi:10.1594/GFZ.WSM.Rel2008.
549 Kanamori, H., and D. L. Anderson (1975). Theoretical basis of some empirical relations in
550 seismology, *Bull. Seismol. Soc. Amer.*, **65**, 1073-1095.

551 Kastelic, V., P. Vannoli, P. Burrato, U. Fracassi, M. Tiberti, and G. Valensise (2013).
552 Seismogenic sources in the Adriatic Domain, *Marine and Petroleum Geology* **42**, 191-213,
553 doi: 10.1016/j.marpetgeo.2012.08.002.
554 Kennett, B.L.N. (2005). Seismological Tables: ak135, Research School of Earth Sciences, The
555 Australian National University, pp. 290.
556 Levret, A., J. C. Backe, and M. Cushing (1994). Atlas of macroseismic maps for French
557 earthquakes with their principal characteristics, *Natural Hazards* **10**, 19-46.
558 Lolli, B., P. Gasperini, and G. Vannucci (2014). Empirical conversion between teleseismic
559 magnitudes (m_b and M_s) and moment magnitude (M_w) at the Global, Euro-Mediterranean and
560 Italian scale, *Geophysical Journal International* **199**, 805-828, doi: 10.1093/gji/ggu264.
561 Lomax, A. (2005). A reanalysis of the hypocentral location and related observations for the great
562 1906 California earthquake, *Bulletin of the Seismological Society of America* **95**, 861-877,
563 doi: 10.1785/0120040141.
564 Macchiavelli C., S. Mazzoli, A. Megna, F. Saggese, S. Santini, and S. Vitale (2012). Applying
565 the Multiple Inverse Method to the analysis of earthquake focal mechanism data: new insights
566 into the active stress field of Italy and surrounding regions, *Tectonophysics* **580**, 124-149, doi:
567 10.1016/j.tecto.2012.09.007.
568 Maesano, F. E., G. Toscani, P. Burrato, F. Mirabella, C. D'Ambrogi, and R. Basili (2013).
569 Deriving thrust fault slip rates from geological modeling: examples from the Marche coastal
570 and offshore contraction belt, Northern Apennines, Italy, *Marine and Petroleum Geology* **42**,
571 122-134, doi: 10.1016/j.marpetgeo.2012.10.008.
572 Malinverno, A., and W. B. F. Ryan (1986). Extension in the Tyrrhenian Sea and shortening in
573 the Apennines as result of arc migration driven by sinking of the lithosphere, *Tectonics* **5**, no.
574 2, 227-245.
575 Margottini, C., N. N. Ambraseys, and A. Screpanti (1993). *La magnitudo dei terremoti italiani*
576 *del XX Secolo*, E.N.E.A. Internal Publication, Rome, 57 pp.

577 Mazzoli, S., C. Macchiavelli, and A. Ascione (2014). The 2013 Marche offshore earthquakes:
578 new insights into the active tectonic setting of the outer northern Apennines, *Journal of the*
579 *Geological Society*, doi: 10.1144/jgs2013-091.
580 Michelini, A., B. De Simoni, A. Amato, and E. Boschi (2005). Collecting, digitizing, and
581 distributing historical seismological data. *EOS Transactions, American Geophysical Union*
582 **86**, no. 28, 261; doi:10.1029/2005EO280002.
583 Mucciarelli, M., and P. Tiberi (Editors) (2007). *Scenari di pericolosità sismica della fascia*
584 *costiera marchigiana. La microzonazione sismica di Senigallia*, Regione Marche-Istituto
585 Nazionale di Geofisica e Vulcanologia, Tecnoprint srl, Ancona, 316 pp.
586 Oddone, E. (1930). Sul terremoto delle Province Ancona e Pesaro avvenuto il di 30 ottobre
587 1930, *Bollettino Società Sismologica Italiana* **XXIX** , 115-140.
588 Okada, Y. (1985). Surface deformation due to shear and tensile faults in a half-space, *Bulletin of*
589 *the Seismological Society of America* **75**, 1135-1154.
590 Pasarić, M., B. Brizuela, L. Graziani, A. Maramai, and M. Orlić (2012). Historical tsunamis in
591 the Adriatic Sea, *Natural Hazards* **61**, 281-316, doi: 10.1007/s11069-011-9916-3.
592 Pasolini, C., D. Albarello, P. Gasperini, V. D'Amico, and B. Lolli (2008). The attenuation of
593 seismic intensity in Italy, Part II: Modeling and validation, *Bulletin of the Seismological*
594 *Society of America* **98**, 692-708.
595 Pino, N. A., B. Palombo, G. Ventura, B. Perniola, and G. Ferrari (2008). Waveform modeling of
596 historical seismograms of the 1930 Irpinia earthquake provides insight on ''blind'' faulting in
597 Southern Apennines (Italy), *Journal of Geophysical Research* **113**, B05303, doi:
598 10.1029/2007JB005211.
599 Pino, N. A., A. Piatanesi, G. Valensise, and E. Boschi (2009). The 28 December 1908 Messina
600 Straits Earthquake (Mw 7.1): A Great Earthquake throughout a Century of Seismology,
601 *Seismological Research Letters* **80**, no. 2, 243-259, doi: 10.1785/gssrl.80.2.243.

602 Pondrelli, S., A. Morelli, G. Ekström, S. Mazza, E. Boschi, and A. M. Dziewonski (2002).
603 European-Mediterranean regional centroid-moment tensors: 1997-2000, *Physics of the Earth*
604 *and Planetary Interiors* **130**, 71-101.
605 Pondrelli, S., S. Salimbeni, A. Morelli, G. Ekström, L. Postpischl, G. Vannucci, and E. Boschi
606 (2011). European-Mediterranean Regional Centroid Moment Tensor Catalog: solutions for
607 2005-2008, *Physics of the Earth and Planetary Interiors* **185**, 74-81, doi:
608 10.1016/j.pepi.2011.01.007.
609 Postpischl, D. (Editor) (1985). *Atlas of isoseismal maps of Italian earthquakes*, Progetto
610 Finalizzato Geodinamica, Quaderni della Ricerca Scientifica, 114, 2A, Roma, 166 pp., 64 tav.
611 Rock, N. M. S. (1988). *Numerical Geology*, Springer-Verlag, Berlin, 427 pp.
612 Scognamiglio, L., E. Tinti, and A. Michelini (2009). Real-Time Determination of Seismic
613 Moment Tensor for the Italian Region, *Bulletin of the Seismological Society of America* **99**,
614 no. 4, 2223-2242, doi: 10.1785/0120080104.
615 Scrocca, D. (2006). Thrust front segmentation induced by differential slab retreat in the
616 Apennines (Italy), *Terra Nova* **18**, 154-161, doi: 10.1111/j.1365-3121.2006.00675.x.
617 Sieberg, A. (1931). Erdebeben, in *Handbuch der Geophysik* B. Gutenberg (Editor), 4, Gebrüder
618 Borntraeger, Berlin, 552-554.
619 Stich, D., J. Batllo, R. Macia, P. Teves-Costa, and J. Morales (2005). Moment tensor inversion
620 with single-component historical seismograms: The 1909 Benavente (Portugal) and Lambesc
621 (France) earthquakes, *Geophysical Journal International* **162**, 850-858, doi: 10.1111/j.1365-
622 246X.2005.02680.x.
623 Valensise, G., and D. Pantosti (2001a). The investigation of potential earthquake sources in
624 peninsular Italy: A review, *Journal of Seismology* **5**, 287-306.
625 Valensise, G., and D. Pantosti (Editors) (2001b). Database of potential sources for earthquakes
626 larger than M 5.5 in Italy, *Annali di Geofisica*, Supplement to vol. **44**, no. 4, 180 pp., with
627 CD-ROM.

628 Vannoli, P., R. Basili, and G. Valensise (2004). New geomorphic evidence for anticlinal growth
629 driven by blind-thrust faulting along the northern Marche coastal belt (central Italy), *Journal*
630 *of Seismology* **8**, 297-312.
631 Vannoli, P., P. Burrato, U. Fracassi, and G. Valensise (2012). A fresh look at the seismotectonics
632 of the Abruzzi (Central Apennines) following the 6 April 2009 L'Aquila earthquake (Mw
633 6.3), *Italian Journal of Geosciences* **131**, no. 3, 309-329, doi:10.3301/IJG.2012.03.
634 Vannoli P., P. Burrato, and G. Valensise (2014). The seismotectonics of the Po Plain (northern
635 Italy): tectonic diversity in a blind faulting domain, *Pure and Applied Geophysics*, doi:
636 10.1007/s00024-014-0873-0.
637 Vannucci, G., and P. Gasperini (2003). A database of revised fault plane solutions for Italy and
638 surrounding regions, *Computers & Geosciences* **29**, 903-909.
639 Vannucci, G., and P. Gasperini (2004). The new release of the database of earthquake
640 mechanisms of the Mediterranean area (EMMA Version 2), *Annals of Geophysics* **47**, 307-
641 334.
642 Vannucci G., P. Imprescia, and P. Gasperini (2010). Deliverable n. 2 of the UR2.05 in the
643 INGV-DPC S1 project (2007-2009). INGV-DPC Internal report and database.
644 Villaseñor, A., and E. R. Engdahl (2005). A digital hypocenter catalog for the International
645 Seismological Summary, *Seismological Research Letters* **76**, 554-559.
646 Wells, D. L., and K. J. Coppersmith (1994). New empirical relationships among magnitude,
647 rapture length, rupture width, rupture area, and surface displacement, *Bulletin of the*
648 *Seismological Society of America* **84**, 974-1002.
649

Full mailing address for each author

Paola Vannoli: paola.vannoli@ingv.it

Gianfranco Vannucci: gianfranco.vannucci@ingv.it

Fabrizio Bernardi: fabrizio.bernardi@ingv.it

Barbara Palombo: barbara.palombo@ingv.it

Graziano Ferrari: graziano.ferrari@ingv.it

Tables

Table 1. Summary of the contributions of Instrumental (I), Macroseismic (M) and Geological (G) data and methods for determining the geometric and kinematics parameters of the source of the 30 October 1930 *Senigallia* earthquake.

Parameter	Data type	Method(s)
Location	I	Analysis of seismograms and bulletins.
	M	Analysis of intensity distribution.
	G	Analysis of geophysical profiles and, if the source is located on land, of the state of deformation of fluvial and coastal terraces.
Magnitude	I	a) Analysis of seismograms; b) Estimated from focal mechanism.
	M	Analysis of intensity distribution based on the attenuation equation of Pasolini *et al*. (2008).
	G	Calculated using empirical relationships between magnitude and fault size.
Depth	I	Fixed in the focal mechanism.
	M	Analysis of geographical intensities distribution. The estimate however is not reliable.
	G	Analysis of geological sections across the active fault system.
Length	I	*Undetermined*
	M	Calculated from magnitude, according to Wells and Coppersmith (1994).
	G	Analysis of a) geological sections; b) the area of warped alluvial and coastal terraces.
Width	I	*Undetermined*
	M	Calculated from magnitude, according to Wells and Coppersmith (1994).
	G	Analysis of a) geological sections; b) the area of warped alluvial terraces.
Strike	I	From focal mechanism.
	M	Calculated from intensity distribution: weighted axial mean of the distribution of the axial orientations of sites with higher intensities.
	G	Analysis of a) strike of anticline; b) modeling of geological data.
Dip	I	From focal mechanism.
	M	*Undetermined*
	G	Analysis of geological sections across the active fault system.
Rake	I	From focal mechanism.
	M	*Undetermined*
	G	Inferred from geological structures and seismological context.

Undetermined indicates that the specific parameter cannot be determined with the given method/data.

Table 2. Macroseismic parameters obtained from the intensity dataset using different methods supplied by BOXER.

Method #	LatE (± bst; ± frm, in km)	LonE (± bst; ± frm, in km)	Offshore/ Onshore	M (± bst; ± frm)
0	43.659 (3.818; 4.154)	13.331 (6.173; 6.189)	E	5.80 (0.07; 0.1)
1	43.643 (2.219; 2.29)	13.364 (2.849; 2.286)	E	5.80 (0.02; 0.1)
2	43.642 (2.394; 2.44)	13.363 (2.829; 2.315)	E	5.80 (0.02; 0.1)
3	43.642 (2.441; 2.534)	13.363 (2.808; 2.314)	E	5.80 (0.02; 0.1)
4	43.642 (2.810; 3.278)	13.363 (2.937; 2.321)	E	5.80 (0.02; 0.1)
5	43.750 (2.398; 2.331)	13.446 (3.339; 3.372)	S	5.83 (0.02; 0.1)
6	43.812 (4.061; 4.419)	13.504 (4.414; 4.100)	S	5.85 (0.03; 0.1)

Key: (LatE), (LonE), epicentral latitude and longitude; (M), magnitude with associated bootstrap (bst) and formal (frm) uncertainties (in km) at 90% confidence level (Gasperini *et al.*, 2010). (S) or (E) indicate whether the epicentral location falls offshore or onshore (Fig. 5). Notice that the magnitude is fairly stable for offshore and onshore solutions.

675 **Table 3.** Data and stations used for earthquake location.

676

Station code	Lat (deg)	Lon (deg)	Distance (km)	P phase	S phase	Arrival time
VEN	45.433	12.333	195	P		07:13:27
VEN	45.433	12.333	195		SS (nu)	07:14:04
PAD	45.409	11.886	211	P		07:13:27
TRV	45.667	12.183	223	P		07:13:28
TRV	45.667	12.183	223		S (nu)	07:13:52
RDP	41.758	12.717	242	P		07:13:30
RDP	41.758	12.717	242		SS	07:14:06
LJU	46.044	14.527	256	P		07:13:34
LJU	46.044	14.527	256		sSS (nu)	07:14:16
ZAG	45.829	15.994	296	P		07:13:39
ZAG	45.829	15.994	296		sSS	07:14:22
CSM	40.750	13.900	349	pP		07:13:54
CSM	40.750	13.900	349		S	07:14:24
GRA	47.077	15.448	389	P		07:13:51
GRA	47.077	15.448	389		SSSS	07:14:51
BAI	41.107	16.879	417	Pg (nu)		07:14:07
BAI	41.107	16.879	417		SSSS	07:14:59
ZUR	47.369	8.580	543	P (nu)		07:14:04
ZUR	47.369	8.580	543		S	07:15:08
MAR	43.305	5.394	651	pP (nu)		07:14:27
MAR	43.305	5.394	651		SS	07:15:41
CRL	39.133	8.317	678	pP (nu)		07:14:30
CRL	39.133	8.317	678		Sg	07:15:55
KRL	49.011	8.412	689	P		07:14:27
KRL	49.011	8.412	689		S (nu)	07:15:45
CHE	50.079	12.376	695	Pg		07:14:46
CHE	50.079	12.376	695		SS (nu)	07:15:49
JEN	50.952	11.583	800	P		07:14:41
JEN	50.952	11.583	800		S (nu)	07:16:06
GTT	51.546	9.964	892	P (nu)		07:14:50
GTT	51.546	9.964	892		SS	07:16:35
DBN	52.102	5.177	1101	pP (nu)		07:15:23
DBN	52.102	5.177	1101		SS	07:17:24
OXD	51.767	-1.250	1401	P		07:15:55
OXD	51.767	-1.250	1401		SS (nu)	07:18:32
ALM	36.853	-2.460	1553	pP		07:16:21
ALM	36.853	-2.460	1553		SS	07:19:04
BID	53.400	-3.067	1604	P		07:16:20
BID	53.400	-3.067	1604		S (nu)	07:19:06

SEV	44.545	33.668	1610	P		07:16:21
CRT	37.190	-3.598	1616	P		07:16:21
CRT	37.190	-3.598	1616		sSS	07:19:27
SIM	44.949	34.116	1642	P		07:16:26
YAL	44.488	34.155	1649	P		07:16:24
UPP	59.858	17.627	1800	P		07:16:43
UPP	59.858	17.627	1800		S (nu)	07:19:46
PUL	59.767	30.317	2101	P		07:17:16
PUL	59.767	30.317	2101		S (nu)	07:20:41
HLW	29.858	31.342	2218	P		07:17:29
HLW	29.858	31.342	2218		S (nu)	07:21:11
TNT	43.667	-79.400	7015		S	07:31:55
CHK	41.789	-87.599	7669		S	0,315625

677

678 Bulletin data: station code and coordinates, epicentral distance, detected P and S phases (nu= not

679 used), arrival time.

680

Table 4. Seismograms used for Moment Tensor computation and associated instrumental constants.

Station code	Lat (deg)	Lon (deg)	Distance (km)	It	Comp.	T_0	Damp.	Magn.	Pol	MT
ALI	38.355	-0.487	1316	M	E-W	10	0.28	120		*
ATH	37.972	23.717	1083	M	Z				*	
ATH	37.972	23.717	1083	M	N-S	5.8	0.46	80		*
ATH	37.972	23.717	1083	M	E-W	5.8	0.46	80	*	
CHE	50.079	12.376	695	M	E-W	20	0.53	110	*	*
COP	55.685	12.433	1316	E	E-W	12.7;12.5	0.4;0.4	796		*
DBN	52.102	5.177	1101	E	E-W	25.0;25.0	0.4;0.4	245	*	*
DBN	52.102	5.177	1101	E	N-S	24.4;24.4	0.4;0.4	245	*	
FBR	41.416	2.125	964	M	E-W	9.4	0.42	71		*
FBR	41.416	2.125	964	M	N-S	9.7	0.39	71	*	
HLW	29.858	31.342	2218	M	E-W	12	0.69	250		*
HLW	29.858	31.342	2218	M	Z				*	
JEN	50.952	11.583	800	M	N-S	8.6	0.26	235		*
JEN	50.952	11.583	800	M	E-W				*	
KEW	51.468	-0.313	1329	E	N-S	24.8;25.2	0.4;0.4	880		*
KEW	51.468	-0.313	1329	E	E-W	24.8;25.2	0.4;0.4	880	*	*
PCN	45.050	9.667	327	M	N-S	5	0.5	243	*	
PCN	45.050	9.667	327	M	Z				*	
PCN	45.050	9.667	327	M	E-W	12.5	0.4	2.43	*	
PRA	50.070	14.433	694	M	N-S	9.8	0.5	212	*	
STR	48.579	7.763	682	E	E-W	22.2;22.2	0.4;0.4	460	*	*
UCC	50.798	4.359	1029	E	Z	11.5;8.0	0.4;0.4	880	*	
ZAG	45.829	15.994	296	M	N-S	9	0.37	200	*	
ZAG	45.829	15.994	296	M	E-W	5	0.5	50	*	
ZUR	47.369	8.580	543	M	N-S	5.1	0.33	198	*	
ZUR	47.369	8.580	543	M	E-W	5	0.5	50	*	

Seismogram data: station code and coordinates, epicentral distance, instrument type (It: M = mechanical, E = electromagnetic), instrument component (Comp.), constants (T_o = free period, Damp. = damping, Magn. = magnification). For electromagnetic instruments the table supplies the free period and damping of the seismometer and galvanometer, respectively. The last two columns indicate if the seismogram was used for polarity reading (Pol) and/or Moment Tensor inversion (MT).

Figure captions

Figure 1. Aerial photo of the Rione Porto (Senigallia). Notice the collapse of roofs and the widespread damage to buildings. The church of Santa Maria del Ponte al Porto and its unsafe bell tower is seen in the foreground. The Portici Ercolani are shown on the left side of the image (on the right bank of the Misa River). This rare photo was taken by the air squadrons of the 20th *Stormo* of the *Aeronautica Militare Italiana* immediately after the earthquake.

Figure 2. Macroseismic intensities of the 30 October 1930, *Senigallia* earthquake (CPTI11, see Data and Resources Section) expressed with the MCS scale (Sieberg, 1931). The inset shows all available intensities. Arrows in inset show the two localities (A: Ancona, B: Bakar) where the tsunami was observed (CFTI4Med, see Data and Resources Section; Pasarić *et al.*, 2012).

Figure 3. Geological sketch of the study area showing Composite Seismogenic Sources (shown by gray dotted areas) and the Individual Seismogenic Source (*Senigallia* GS is shown by the black individual source) from the DISS database (seeData and Resources Section) and selected structural elements (Bigi *et al.*, 1992, modified). Details of the P and T axes (Vannucci and Gasperini 2003; 2004) are given in Table S1 of the *Electronic supplement*. Contours show the zone of expected uplift (+ 12 cm of maximum uplift) and subsidence (–) based on the Okada (1985) elastic dislocation code. Key: CL: Conca Line (Elmi *et al.*, 1987); MSPL: Monte San Vicino-Polverigi Line (a set of NE-SW faults which includes the Esino Line; Coltorti and Nanni, 1987).

Figure 4. Seismicity and geodynamic characteristics of the region. a) Orientation of the maximum horizontal compressive stress (Heidbach *et al*., 2008), horizontal GPS velocity vectors (Devoti *et al*., 2011), and arthquake epicenters from different sources (Villaseñor and

717 Engdahl, 2005; ISS,; CPTI11,; ISC, see Data and Resources Section) for which the M_w was
718 re-evaluated according to the GASP calibration formulas (Gasperini *et al*., 2012, 2013a,
719 2013b; Lolli *et al.*, 2014). The legend shows details of catalogues covering different time
720 periods (ISC, CPTI11, see Data and Resources Section); b) Detail of the seismicity.
721
722 **Figure 5**. Macroseismic source (MS) and macroseismic epicenters obtained from macroseismic
723 intensities of the 1930 earthquake using all methods made available by the BOXER code
724 (Gasperini *et al*., 2010; methods #0-6, see text for further details). The instrumental epicenters
725 made available by the International Seismological Summary (ISS, see Data and Resources
726 Section), by Gutenberg and Richter (GUTE; 1954) and by this study (NLL) are also shown.
727 Uncertainty ellipses (if shown) are plotted at 90% confidence. A rose diagram indicates the
728 stations for 10 degree azimuth sectors used for computing the NLL epicenter.
729
730 **Figure 6**. Summary of the stations used (or not used) for locating the 1930 earthquake by
731 NonLinLoc (Lomax, 2005) and of seismograms used (or not used) to assess the focal
732 mechanism by Moment Tensor inversion and by analyzing first motion polarities. Inset
733 indicates the global stations used (or not used) behind the main panel. See Tables 3 and 4 for
734 details on the stations used.
735
736 **Figure 7**. Power spectra amplitudes of the stations used for MT inversion. Station codes,
737 seismogram directions (E-W/N-S), synthetic (dark and dashed lines) and observed (gray line)
738 power spectra amplitudes are shown. Distance (δ), azimuth (ϕ) and take off angles (ai)
739 between epicenter and stations are also indicated.
740
741 **Figure 8**. Macroseismic (MS) and Geological (GS) sources of the 1930 earthquake, with
742 geometric and kinematics parameters, compared with the preferred plane (black thick-line)

743 resulting from the Moment Tensor inversion (MT). The rose diagram shows the azimuth
744 distribution of macroseismic BPDs. Bootstrap (bst), formal (frm) and hessian (hes)
745 uncertainties (Gasperini *et al*., 2010) are shown at 90% confidence (see text for further
746 details).
747

Figures

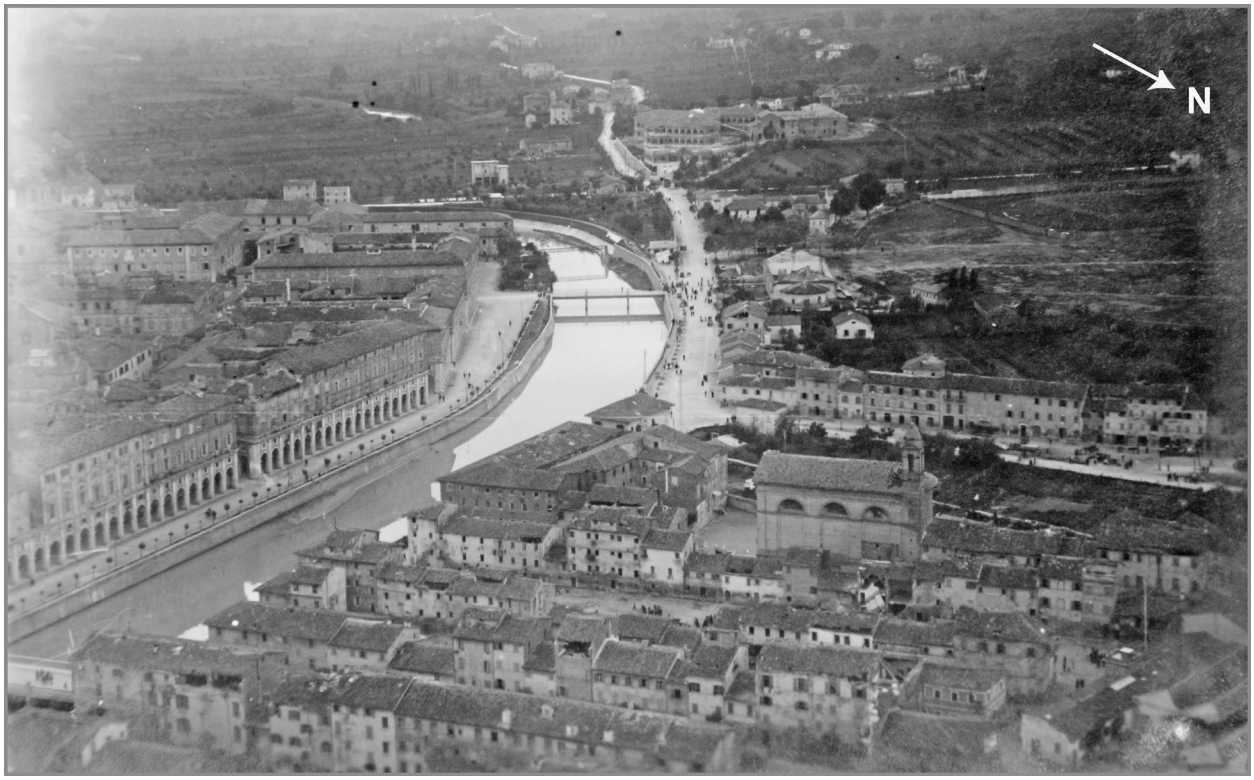

Figure 1. Aerial photo of the Rione Porto (Senigallia). Notice the collapse of roofs and the widespread damage to buildings. The church of Santa Maria del Ponte al Porto and its unsafe bell tower is seen in the foreground. The Portici Ercolani are shown on the left side of the image (on the right bank of the Misa River). This rare photo was taken by the air squadrons of the 20th *Stormo* of the *Aeronautica Militare Italiana* immediately after the earthquake.

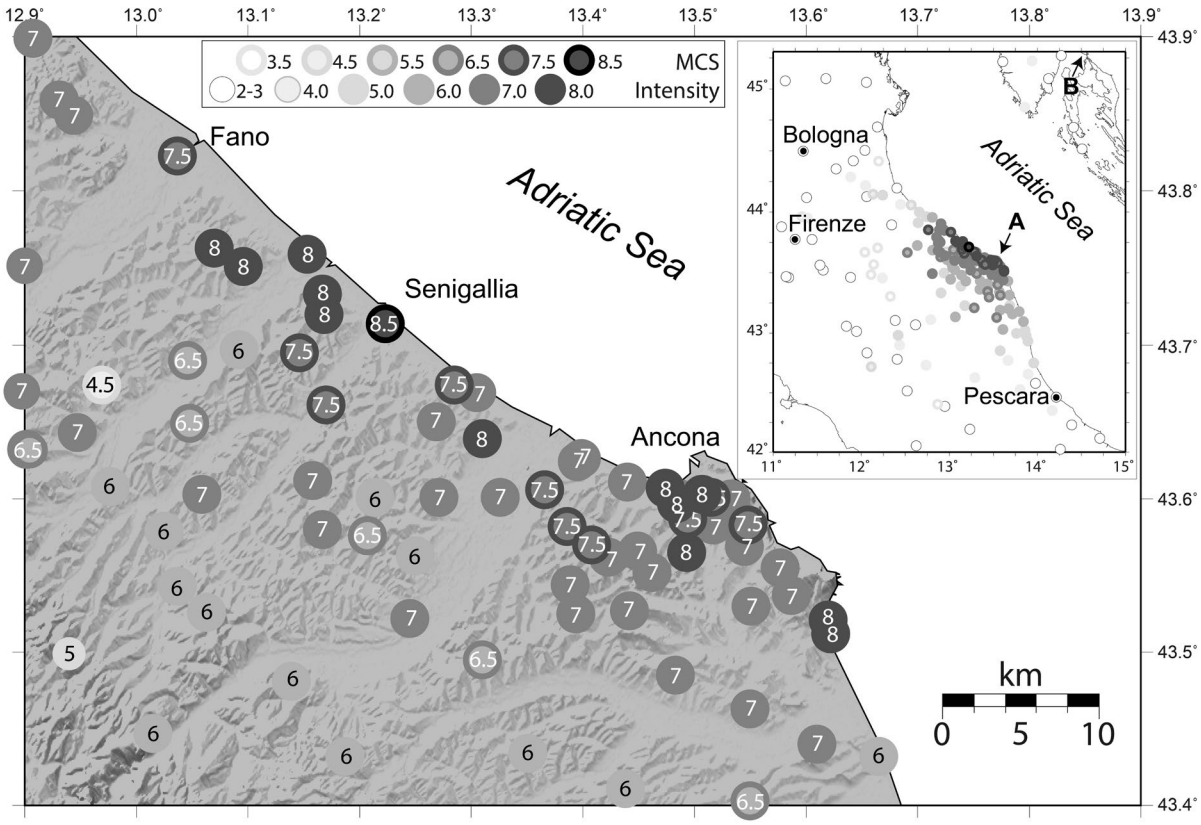

Figure 2. Macroseismic intensities of the 30 October 1930, *Senigallia* earthquake (CPTI11, see Data and Resources Section) expressed with the MCS scale (Sieberg, 1931). The inset shows all available intensities. Arrows in inset show the two localities (A: Ancona, B: Bakar) where the tsunami was observed (CFTI4Med, see Data and Resources Section; Pasarić *et al.*, 2012).

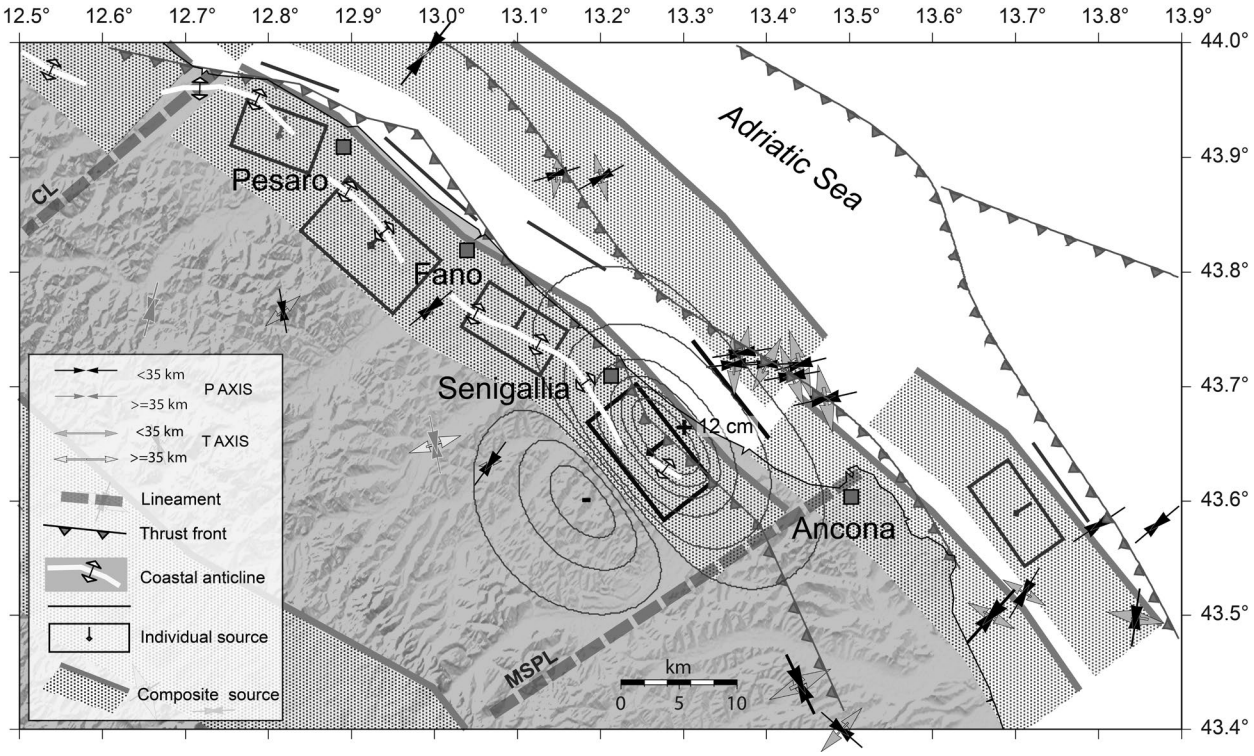

Figure 3. Geological sketch of the study area showing Composite Seismogenic Sources (shown by gray dotted areas) and the Individual Seismogenic Source (*Senigallia* GS is shown by the black individual source) from the DISS database (seeData and Resources Section) and selected structural elements (Bigi *et al.*, 1992, modified). Details of the P and T axes (Vannucci and Gasperini 2003; 2004) are given in Table S1 of the *Electronic supplement*. Contours show the zone of expected uplift (+ 12 cm of maximum uplift) and subsidence (–) based on the Okada (1985) elastic dislocation code. Key: CL: Conca Line (Elmi *et al.*, 1987); MSPL: Monte San Vicino-Polverigi Line (a set of NE-SW faults which includes the Esino Line; Coltorti and Nanni, 1987).

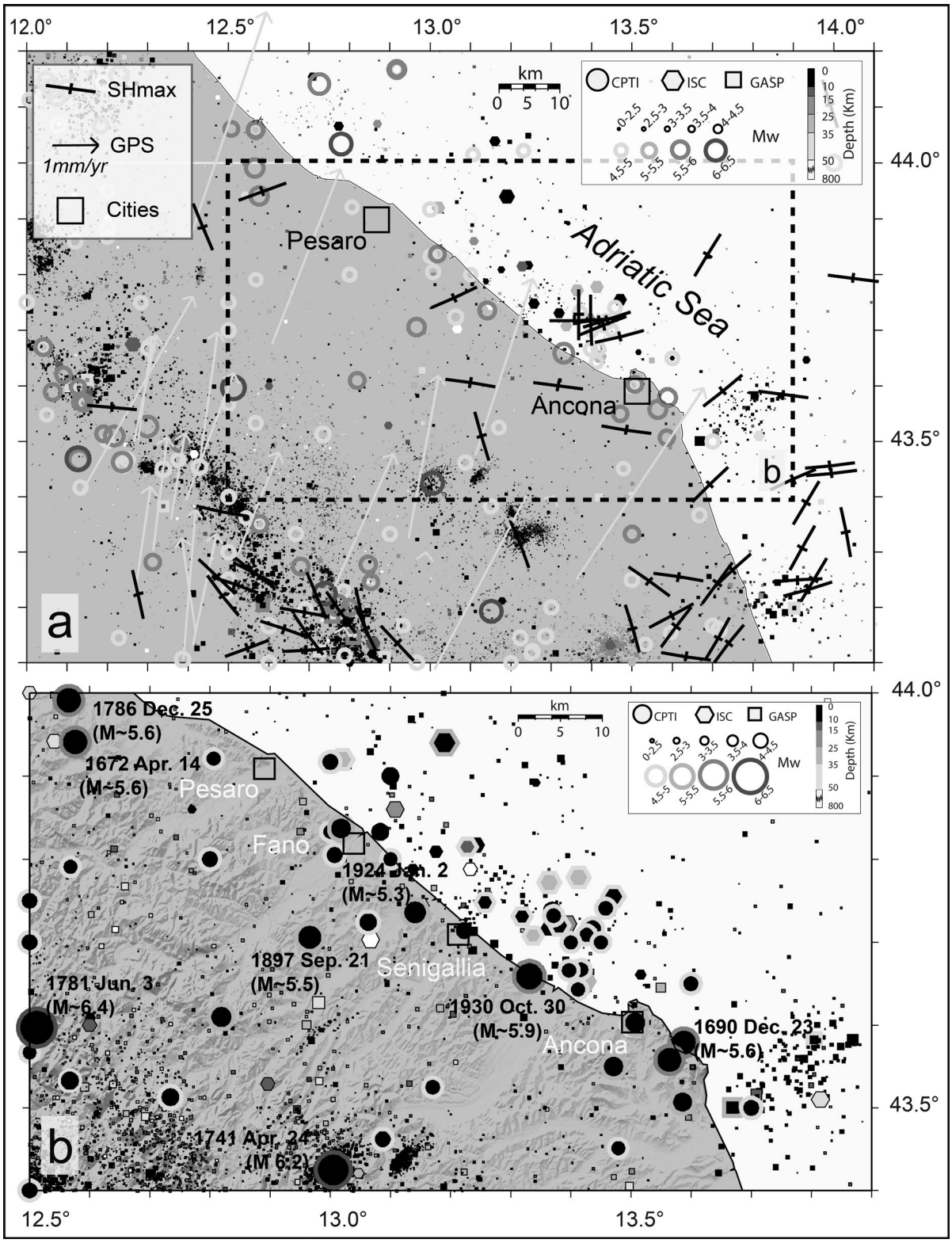

Figure 4. Seismicity and geodynamic characteristics of the region. a) Orientation of the maximum horizontal compressive stress (Heidbach *et al*., 2008), horizontal GPS velocity vectors (Devoti *et al*., 2011), and arthquake epicenters from different sources (Villaseñor and Engdahl, 2005; ISS,; CPTI11,; ISC, see Data and Resources Section) for which the M_w was re-evaluated according to the GASP calibration formulas (Gasperini *et al*., 2012, 2013a,

2013b; Lolli *et al.*, 2014). The legend shows details of catalogues covering different time periods (ISC, CPTI11, see Data and Resources Section); b) Detail of the seismicity.

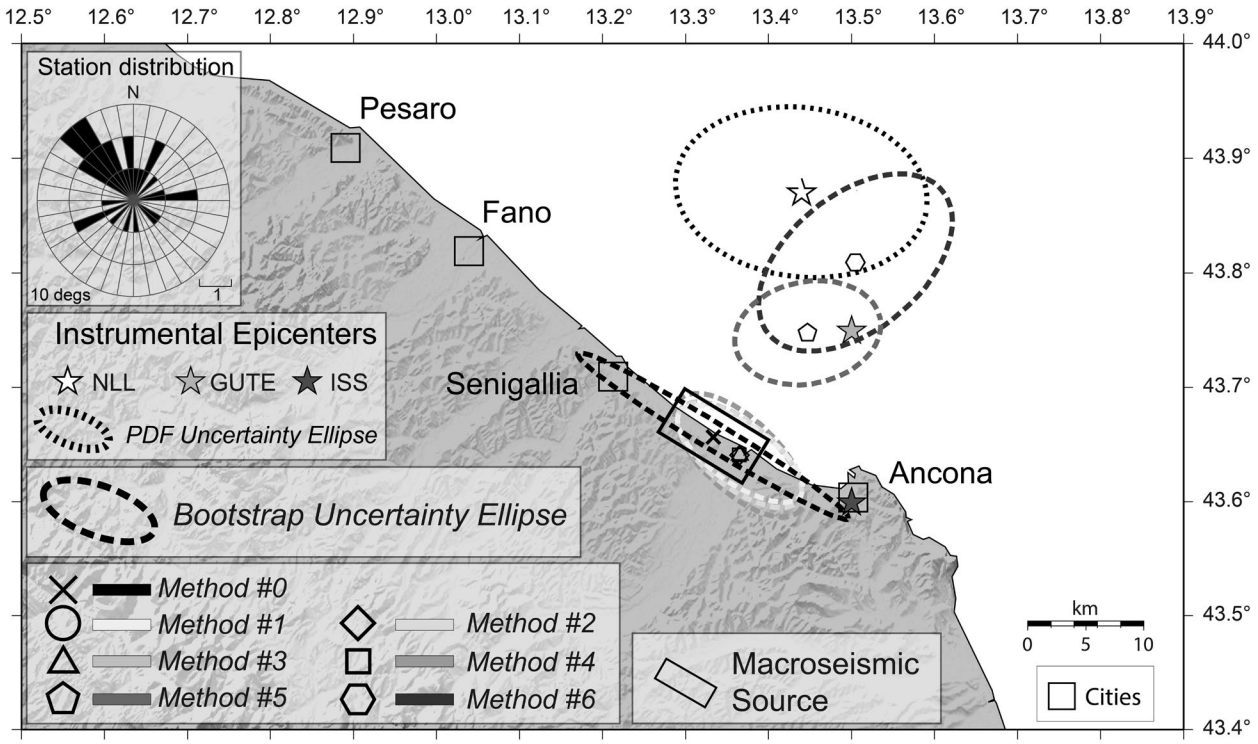

Figure 5. Macroseismic source (MS) and macroseismic epicenters obtained from macroseismic intensities of the 1930 earthquake using all methods made available by the BOXER code (Gasperini *et al*., 2010; methods #0-6, see text for further details). The instrumental epicenters made available by the International Seismological Summary (ISS, see Data and Resources Section), by Gutenberg and Richter (GUTE; 1954) and by this study (NLL) are also shown. Uncertainty ellipses (if shown) are plotted at 90% confidence. A rose diagram indicates the stations for 10 degree azimuth sectors used for computing the NLL epicenter.

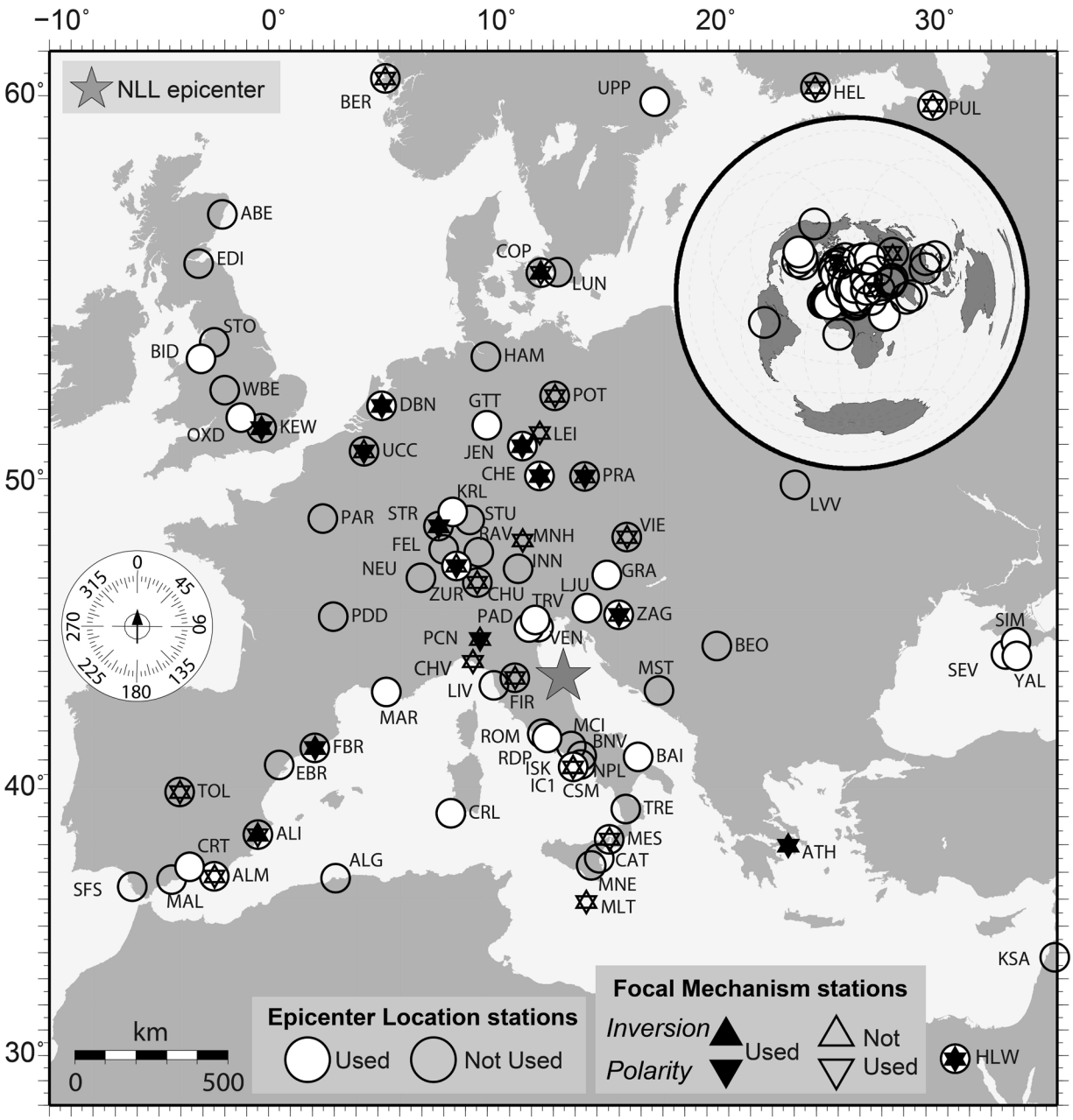

Figure 6. Summary of the stations used (or not used) for locating the 1930 earthquake by NonLinLoc (Lomax, 2005) and of seismograms used (or not used) to assess the focal mechanism by Moment Tensor inversion and by analyzing first motion polarities. Inset indicates the global stations used (or not used) behind the main panel. See Tables 3 and 4 for details on the stations used.

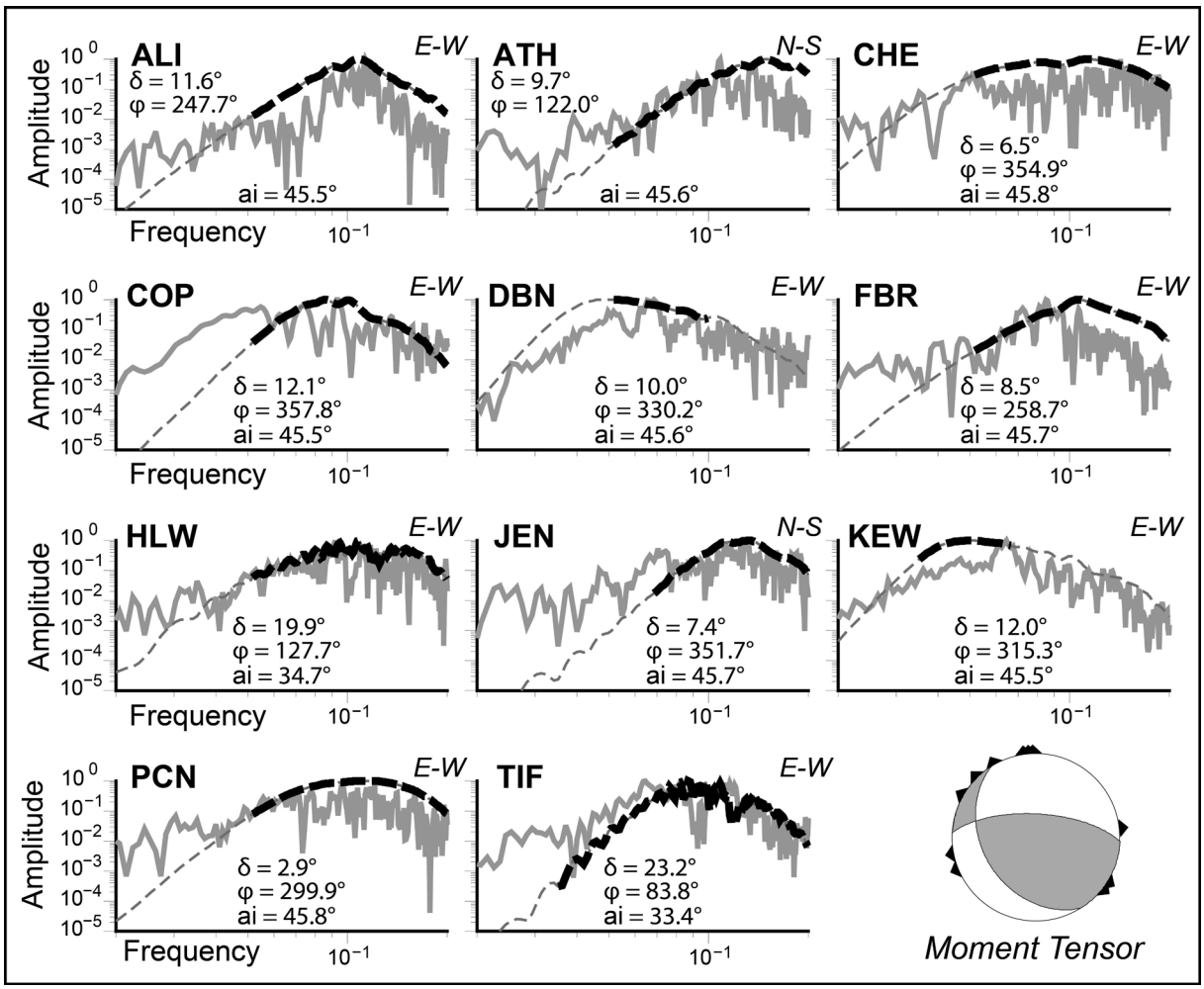

Figure 7. Power spectra amplitudes of the stations used for MT inversion. Station codes, seismogram directions (E-W/N-S), synthetic (dark and dashed lines) and observed (gray line) power spectra amplitudes are shown. Distance (δ), azimuth (ϕ) and take off angles (ai) between epicenter and stations are also indicated.

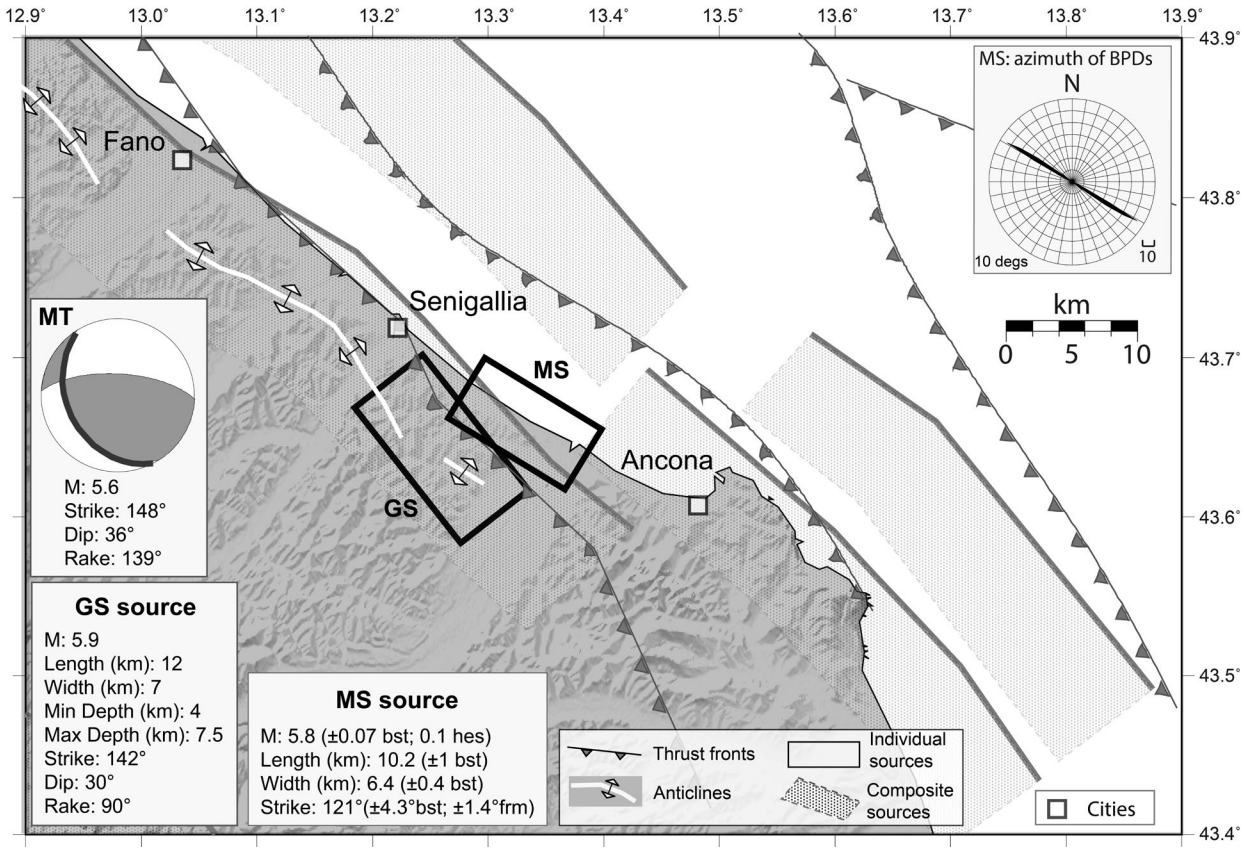

Figure 8. Macroseismic (MS) and Geological (GS) sources of the 1930 earthquake, with geometric and kinematics parameters, compared with the preferred plane (black thick-line) resulting from the Moment Tensor inversion (MT). The rose diagram shows the azimuth distribution of macroseismic BPDs. Bootstrap (bst), formal (frm) and hessian (hes) uncertainties (Gasperini *et al*., 2010) are shown at 90% confidence (see text for further details).